Available online at www.sciencedirect.com
SCIENCE DIRECT®
Finite Elements in Analysis and Design 40 (2003) 213–237
FINITE ELEMENTS IN ANALYSIS AND DESIGN
www.elsevier.com/locate/finel

Estimation of the plastic volume fraction from a linear-elastic finite element analysis

A.C.A. Ramsay*,[1]

PCA Engineers Limited, Homer House, Sibthorp Street, Lincoln LN5 7SB, UK

Received 2 July 2002; received in revised form 12 September 2002; accepted 23 September 2002

Abstract

The plastic volume fraction is one of a range of parameters used in the design of rotating components that are subjected to an overspeeding cycle as part of the manufacturing process. Overspeeding is carried out in order to impart favourable residual compressive stresses and thereby improve the component's fatigue life. However, the amount of material that becomes plastic during overspeeding needs to be controlled carefully if pre-machined manufacturing tolerances are to be maintained. The plastic volume fraction expresses the volume of material in which yield has occurred as a fraction of the total volume, the actual value of which may only be determined through non-linear plastic analysis. The complexity and associated cost of such analyses are of such a level that a linear-elastic approximation to the plastic volume fraction is often used in lieu of the exact quantity. This paper presents a scheme for estimating the plastic volume fraction as a post-processing operation conducted on the results of a three-dimensional linear-elastic finite element analysis. The performance of the scheme is evaluated through numerical examples using element types typically found in commercial finite element codes. In addition to considering how the scheme is able to approximate the linear-elastic plastic volume fraction, plastic analysis is used to illustrate the way in which this quantity approximates the actual plastic volume fraction. The paper concludes with the analysis of a centrifugal impeller; a component drawn from the author's own field of interest. This analysis enables the various strands of the paper to be brought together and provides an example through which it is possible to discuss suitable limiting values for the plastic volume fraction. The examples indicate a plastic volume fraction of 0.05 to be a reasonable limiting value for the linear-elastic approximation adopted in this paper.

Keywords: Plastic volume fraction; Finite element analysis; Stress analysis; Centrifugal impellers; Overspeeding; Fatigue analysis; Rotating components; Rotating disc; Turbomachinery design

* Fax: +44-1522-545-830.
E-mail address: angus_ramsay@yahoo.co.uk (A.C.A. Ramsay).
[1] Visiting Research Fellow, Department of Civil & Structural Engineering, The Nottingham Trent University, Nottingham, UK.

0168-874X/03/$ - see front matter © 2002 Elsevier B.V. All rights reserved.
doi:10.1016/S0168-874X(02)00224-X

Nomenclature

a_1, a_2 and a_3	dimensions of rectangular parallelepiped
A	area of generator plane
c	no of nodal stress configurations
d	depth of plastic penetration
D	collection of terms
E	Young's modulus
F	plastic volume fraction
L	normalised applied load
M	applied moment
n	no of sampling points
N	normalised area
p	no of nodes for an element
q	no of nodes where stress $>$ yield
r	radius
R	strain energy fraction
S	normalised yield stress
t	axial thickness of disc
U	strain energy
x_i, y_i and z_i	Cartesian coordinates of node i
v	Poisson's ratio
ρ	density
σ	normal stress
ω	angular velocity

Subscripts

eq	equivalent
h	finite element value
p	at plastic interface or yield surface
i	at inner radius
o	at outer radius
1, 2, and 3	components of principal stress
y	yield value
r	radial component of stress
θ	tangential component of stress

Superscripts

e	elastic
p	plastic
tilde	used to denote a quantity calculated by sampling the FE stress field

1. Introduction

1.1. Background

The impellers of modern centrifugal compressors operate at high rim speeds with consequently large stresses particularly in the bore or central region of the impeller hub or disc. Impeller designers take considerable care, through attention to disc and vane geometry design, to achieve the lowest possible stresses consistent with maintaining structural integrity in service and, in particular, a satisfactory fatigue life [1]. The efforts of the designer to minimise the centrifugal stresses can be usefully assisted by the process known as overspeeding [2,3], the finished or part-finished component is subjected to a short period of high-speed rotation on a purpose-built rig. The speed is selected such that the most highly stressed regions become plastically deformed during the overspeed run and, on deceleration, the release of strain in the surrounding elastic regions leads to favourable residual stresses which may serve to reduce the mean working stress when cycling between speeds and can provide a valuable improvement in the fatigue life of the component.

The degree to which the material yields during the overspeed operation depends upon the centrifugal load which varies with the square of the angular velocity. For impellers that are machined prior to overspeeding, gross plastic deformation needs to be avoided if manufacturing and balancing tolerances are to be maintained. Local yielding in regions of stress concentration, however, is desirable for the reasons outlined above. It is important, therefore, during the design phase of a component, to be able to predict the location and degree to which yield will occur for a given level of overspeed.

Traditionally, such an assessment of yield is performed manually through visual inspection of contour or carpet plots of the relevant stress function derived from a stress analysis typically using the finite element method. Over recent years there has been a move towards the use of automated computational optimisation techniques in the design of centrifugal impellers. These techniques require the rapid assessment of large numbers of competing design variants and for this reason it has become necessary to formalise and to automate the assessment of yield.

A quantity that may be used to assess the degree of yield in competing designs is the *plastic volume fraction* (PVF) and is here given the symbol F. This quantity is defined as the ratio of the volume of material that has yielded to the total volume of material and may only be determined through non-linear plastic analysis. Such analyses are complex and expensive to perform and, as a cheaper, quicker alternative, more suited to use with the automated optimisation application mentioned above, an estimate of the PVF may be derived from the results of a linear-elastic stress analysis. This quantity is called the *plastic volume fraction—elastic* (PVFE) and is given the symbol F^e.

As the PVFE is not generally reported in the output of finite element systems a scheme for calculating this quantity as a post-processing operation has been developed. This paper describes the development of this scheme, evaluating its performance through a number of numerical examples and demonstrating its application through the practical example of a centrifugal impeller. Although the scheme presented in this paper was developed for the turbomachinery industry, it could equally well find application in other fields of structural engineering.

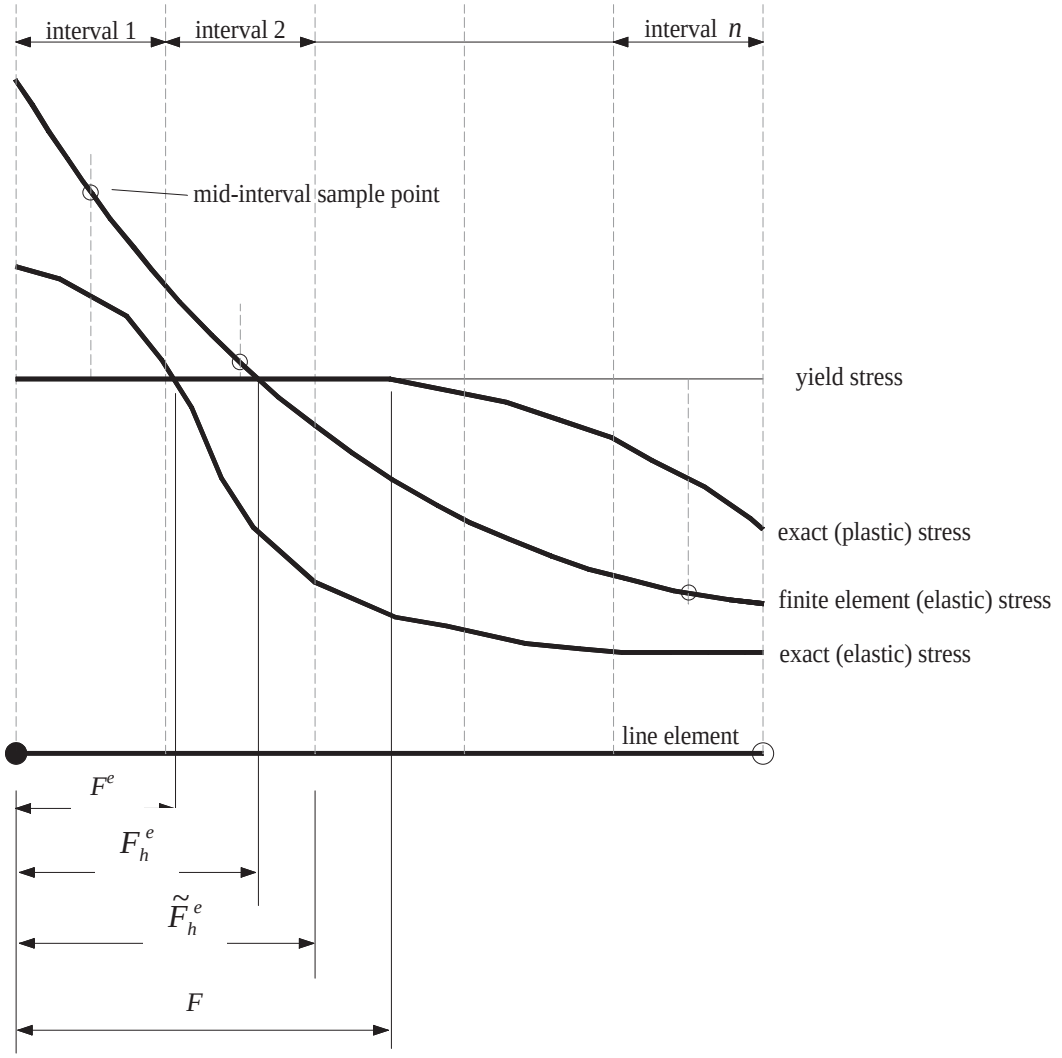

Fig. 1. A simple sampling scheme in 1D ($n = 5$).

2. A simple sampling scheme

A one-dimensional line element and associated stress fields serve as a vehicle to illustrate the definition of the various quantities used in this paper and to demonstrate how they may be calculated.

Consider the one-dimensional element and associated illustrative stress fields shown in Fig. 1.[2] The exact stress field for the problem cannot exceed the yield stress, as shown, and gives the exact plastic volume fraction F. The element is assumed to have uniform cross-sectional area and to be

[2] A convention used in this figure and throughout this paper is that nodes for which the stress exceeds yield are drawn filled.

unit length so that the plastic volume fraction quantities may be marked on the figure as lengths. The linear elastic approximation to the exact stress field, which may exceed the yield stress, is also shown and gives the exact PVFE, F^e. The third stress field shown is the finite element stress field. This stress field will, in general, be different from the other two stress fields and gives the finite element approximation of the PVFE, F_h^e. The purpose of the sampling scheme is to estimate the finite element approximation to the PVFE. This estimate is given the symbol $\tilde{F}_h^e$ and whilst generally being different from F_h^e, any valid sampling scheme should be such that $\tilde{F}_h^e$ is sufficiently close to F_h^e that it may be used in lieu of this quantity.

A simple sampling scheme can be defined in which the element length is divided into n uniform intervals with stress sampling points located at the centre of each interval. The quantity $\tilde{F}_h^e$ is then formed by dividing the summation of the length of the intervals in which the sampled stress exceeds yield, by the total length of the line element. The example highlights the possibility of a difference between the quantities $\tilde{F}_h^e$ and F_h^e. An analysis shows that whenever the difference between the element stress and the yield stress changes sign, an error is introduced into the calculation of the plastic length the maximum value of which can be $\pm$ half the interval length. Thus, for the case where there is only one change in sign over the element, the number of intervals required to guarantee a difference of less than 5% is $n = 10$. The number of sampling points required to provide a similar degree of accuracy in three-dimensions is $n = 10^3$, a figure which is clearly unacceptably large for practical purposes.

In practical finite element analysis F_h^e can be calculated exactly for the so-called constant stress elements such as the three-noded triangle or, in three-dimensions, the four-noded tetrahedron by simply summing up the volume of those elements in which the selected yield criterion is exceeded. In general, and particularly in the analysis of centrifugal impellers, so-called higher-order elements, which admit curved boundaries and linear or quadratic stress variation, are used. For such higher order elements, one could devise a scheme to calculate $\tilde{F}_h^e$ in which representative values of the element stress would be sampled, say at the integration points, and would be weighted with partial element volumes. This method, however, would seem likely to perform badly with the sort of coarse mesh that, for computational speed, is used with the automated optimisation application for which this scheme has been developed. It is important, therefore, that the scheme to be developed account for the variation in stress over the volume of an individual element.

3. The yield surface

As the scheme to be developed needs to take account of the variation of stress in an individual element, it is necessary to describe the yield surface i.e. the interface between regions of the element in which the stress exceeds yield and those in which it is below yield. In the general case, for an element stress field of arbitrary form, the yield surface can be extremely complicated. Even after applying what might be considered appropriate simplifications to the element stress field the problem of explicitly defining this surface remains a difficult one.

In order to reduce the complexity of the yield surface to a manageable level, it will be assumed that the difference between the element stress and the yield stress can change sign no more than once along any edge of an element. In this manner the yield surface can be characterised by the configuration of nodal stresses some of which are above and some of which are below the yield

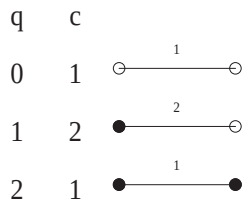

Fig. 2. Nodal stress configurations—1D element ($p = 2$).

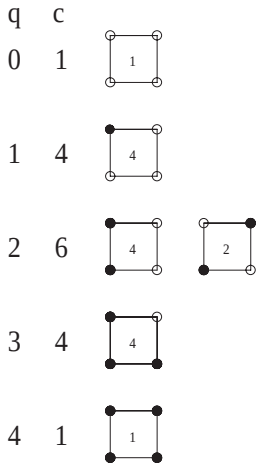

Fig. 3. Nodal stress configurations—2D element ($p = 4$).

stress. For an element with p nodes, the number of configurations of nodal stresses, c, for which q nodal stresses exceed yield is given by the well-known equation (see Ref. [4] for example):

$$c = \binom{p}{q} = \frac{p!}{q!(p-q)!}, \quad q = 0, 1, 2, \ldots, p. \tag{1}$$

The nodal stress configurations corresponding to all permissible values of q for a one-dimensional element with two nodes are shown in Fig. 2. In a manner similar to that just described, the nodal stress configurations for a two-dimensional and for a three-dimensional element are shown, respectively, in Figs. 3 and 4.

Only symmetrically independent configurations are shown in the figures. The total number of such configurations that can be generated by performing a series of rotations about the principal axes of the element is indicated on each figure.

The nature of the yield surface corresponding to a particular nodal stress configuration can be illustrated by joining points on adjacent edges for which the element stress is equal to yield with straight lines. Fig. 5 shows examples of surfaces thus obtained for both two- and three-dimensional elements.

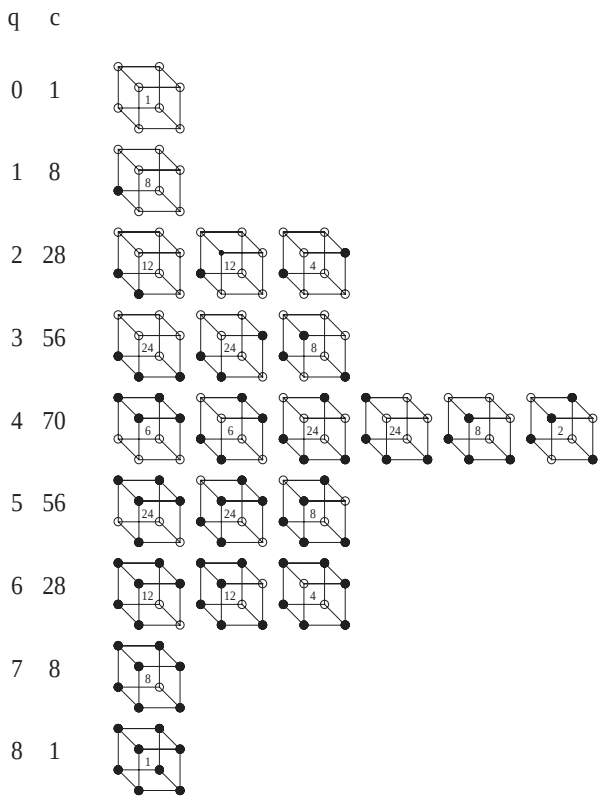

Fig. 4. Nodal stress configurations—3D element ($p = 8$).

4. The plastic volume

The simplified yield surfaces developed in the previous section surround the plastic volume which now needs to be calculated. The shape of the plastic volume will depend on the particular nodal stress configuration and will exhibit a great deal of variability from element to element. A general and efficient procedure for determining the plastic volume can be developed from the realisation that:

(a) the number of nodal stress configurations for a linear tetrahedron is small,
(b) that an analytical expression for the plastic volume occurring with each configuration can be developed for the linear tetrahedron, and,
(c) that other common element shapes, such as the pentahedron and hexahedron are readily subdivided into tetrahedral elements.

The five possible nodal stress configurations and associated plastic volumes for the tetrahedral element are shown in Fig. 6.

With the exception of configuration number 3, the plastic volume is tetrahedral or the complement thereof in the case of configuration number 4 and calculable from the well-known formula (see

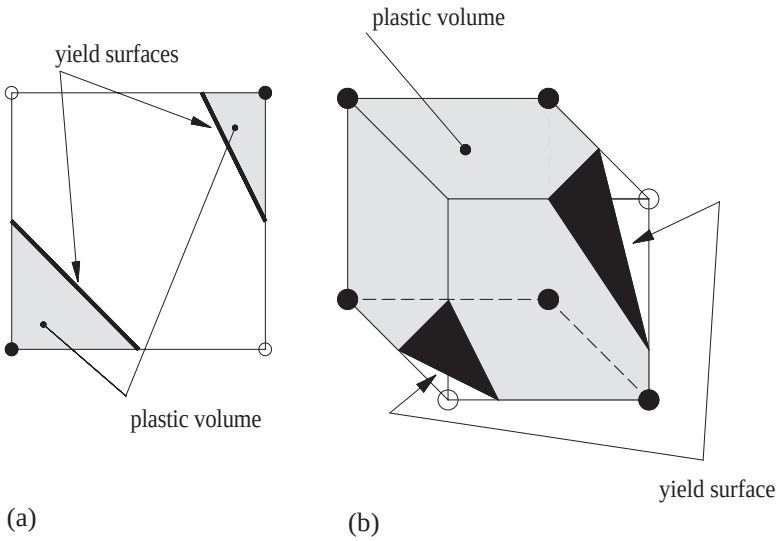

Fig. 5. Example yield surfaces.

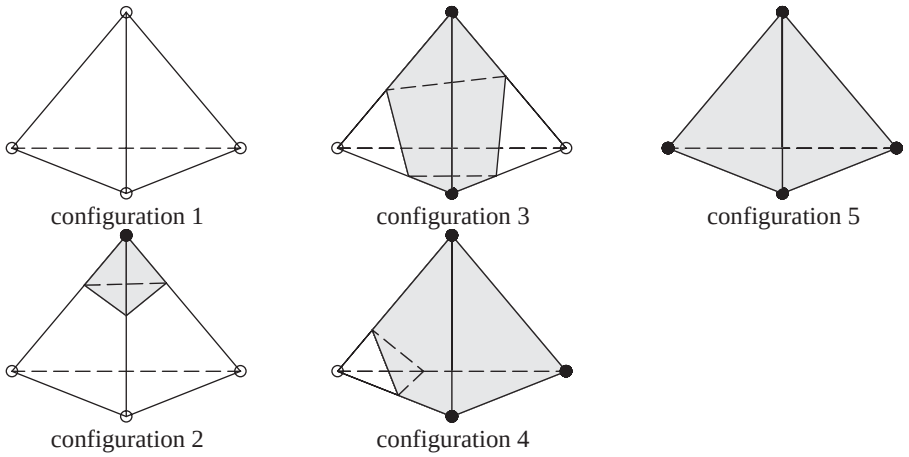

Fig. 6. Plastic volume in a tetrahedron.

Ref. [5] for example):

$$V = \frac{1}{6}\det\begin{bmatrix} 1 & x_1 & y_1 & z_1 \\ 1 & x_2 & y_2 & z_2 \\ 1 & x_3 & y_3 & z_3 \\ 1 & x_4 & y_4 & z_4 \end{bmatrix}, \tag{2}$$

where x_i, y_i and z_i are the co-ordinates of vertex i of the plastic volume.

For configuration number 3 the plastic volume is pentahedral in shape and needs to be sub-divided into two tetrahedra so as to calculate the plastic volume.

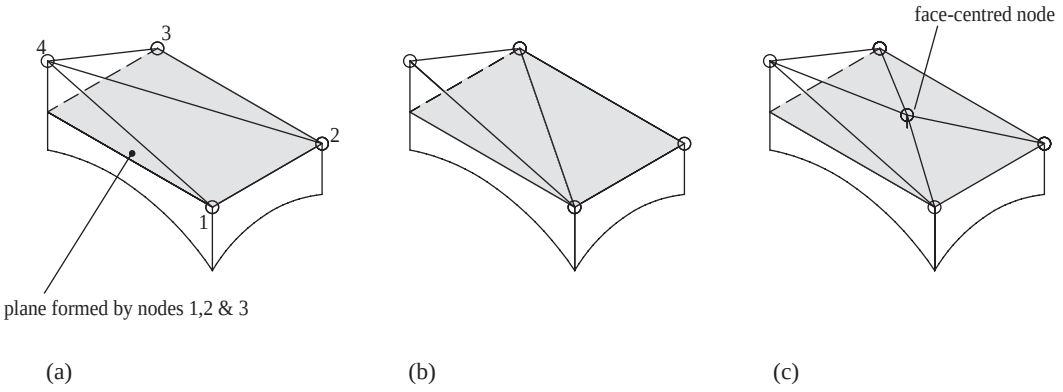

Fig. 7. Invariant sub-division for a quadrilateral face.

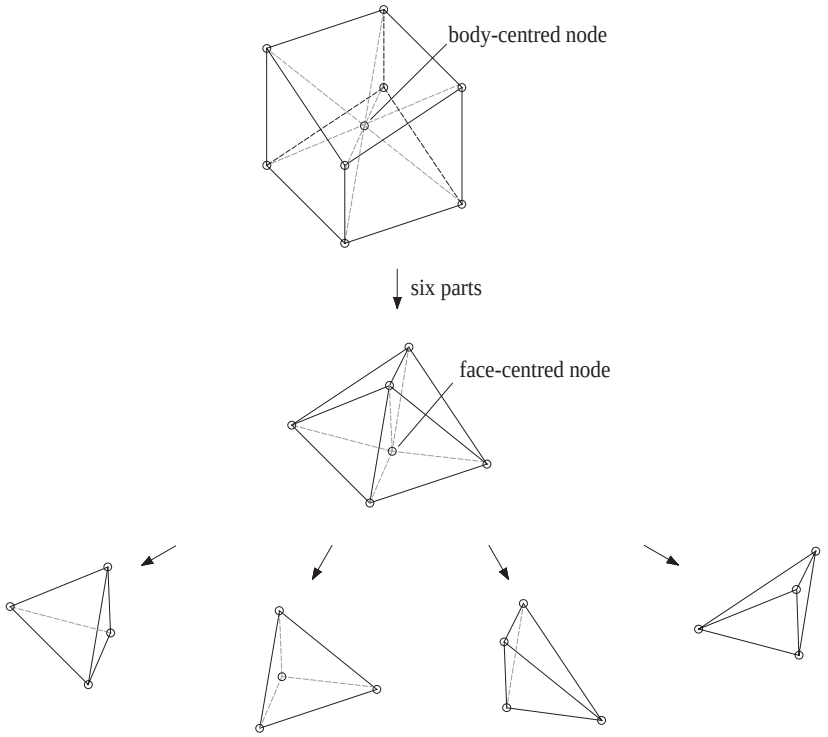

Fig. 8. A systematic way of sub-dividing a hexahedral element into 24 tetrahedra.

Whilst there are a number of ways in which pentahedral and hexahedral elements might be sub-divided into tetrahedral elements, particular attention needs to be given to the way in which quadrilateral faces are sub-divided. In the general case, when all four nodes do not lie in the same plane, the face takes up a shape which can be described as a warped plane [5]. With tetrahedral

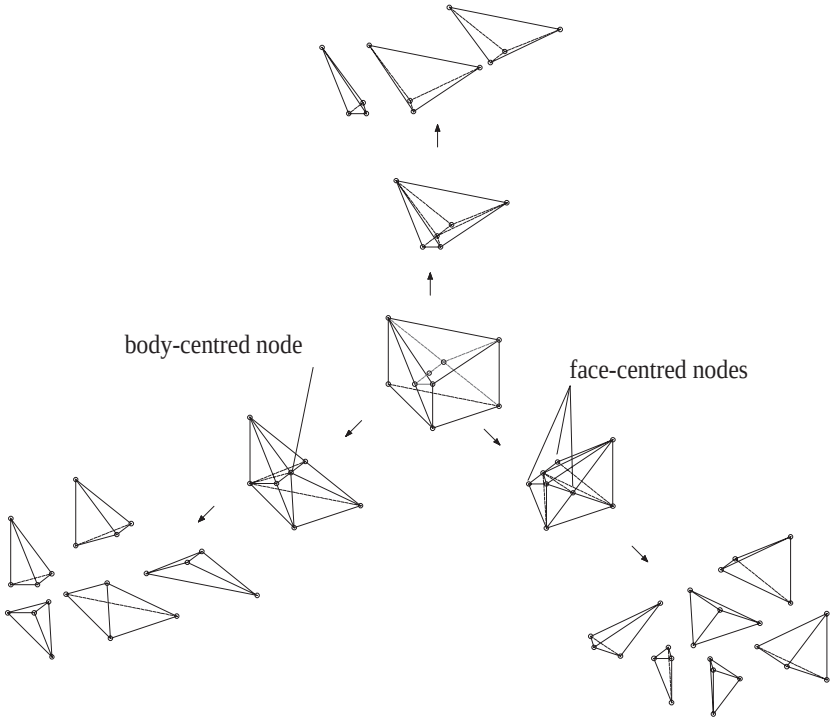

Fig. 9. A systematic way of sub-dividing a pentahedral element into 14 tetrahedra.

sub-division chosen so as to divide the quadrilateral face into two triangles, the volume of the tetrahedra will differ depending on which of the two possible diagonal sub-divisions is chosen—see Fig. 7(a) and (b). This approach to sub-division could lead to erroneous plastic volume calculations and is therefore dismissed. An alternative approach is to carry out tetrahedral sub-division so that quadrilateral faces are divided into four triangles utilising an additional face-centred node. The topologically invariant form of sub-division utilising a face-centred node is shown in Fig. 7(c).

Taking note to ensure that each quadrilateral face is sub-divided in the topologically invariant manner just described, the tetrahedral sub-division chosen for pentahedral and hexahedral elements is shown in Figs. 8 and 9. The co-ordinates of the face-centred and body-centred nodes are determined, respectively, as the average of the four corner nodes defining the quadrilateral face and the 6 or 8 corner nodes defining the pentahedral or hexahedral element.

5. The algorithm

The algorithm used to determine the plastic volume fraction for a mesh of elements and based on the ideas developed in the previous section is shown in the form of a flow chart in Fig. 10. The calculations are performed on elements with linearised geometries i.e. having edges that are straight lines. For higher-order elements with mid-side nodes, the geometry is linearised by assuming the mid-side node to lie at the centre of a line drawn between adjacent corner nodes. The linearisation

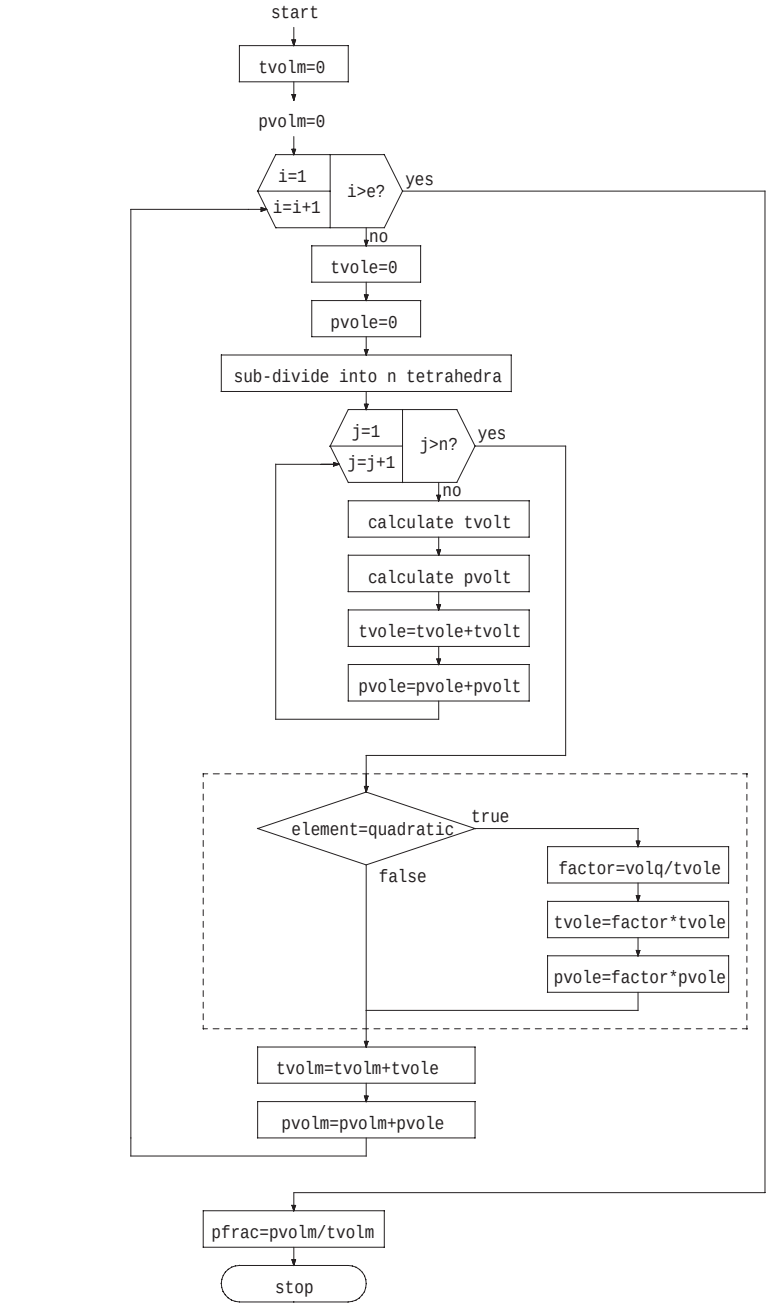

tvolm - total volume of model
pvolm - plastic volume of model
tvole - total volume of element
pvole - plastic volume of element
tvolt - total volume of tetrahedron
pvolt - plastic volume of tetrahedron
volq - total volume of quadratic element
pfrac - plastic volume fraction for model

Fig. 10. Flow chart of algorithm for estimating plastic volume fraction.

of the geometry of quadratic elements introduces a small error in the calculated value of the plastic volume which is accounted for by scaling the linearised value with the ratio of the exact quadratic volume to the linearised volume of the element. The part of the algorithm that deals with this correction is enclosed by a box drawn in dotted lines in the figure.

Each element is sub-divided into tetrahedra the number of which is dependent on the element shape, as already discussed. In order to carry out this sub-division it is necessary to define the positions of face-centred and body-centred nodes and to assign values of stress to these additional nodes. Both the co-ordinates and the stresses of these additional nodes are defined in the same manner. This involves taking the average of the values defining the corner nodes of the face or the corner nodes of the volume.

Following sub-division, the nodal co-ordinates and stresses of each new tetrahedron are passed to a routine in which the total and plastic volume of the tetrahedron are determined. The form of the plastic volume calculation undertaken depends on how many of the nodal stress values exceed the yield stress i.e. on the particular nodal stress configuration. Associated with this calculation is the requirement to determine the positions on the edges of the tetrahedron where the element stress equals the yield stress. These positions are determined based on an assumed linear distribution of stress along element edges between corner nodes.

In order to establish whether or not yield has occurred, a yield criterion is required in which the state of stress, expressed as a single number known as the equivalent stress, σ_{eq}, is compared with the yield stress as established from a simple uniaxial tensile test, σ_y. The equivalent stress commonly used with ductile materials is the von Mises stress [6]. This equivalent stress, can be expressed in terms of the three principal stresses (σ_1, σ_2 and σ_3) as follows:

$$\sigma_{eq} = \frac{1}{\sqrt{2}}\{(\sigma_1 - \sigma_2)^2 + (\sigma_2 - \sigma_3)^2 + (\sigma_3 - \sigma_1)^2\}^{1/2}. \tag{3}$$

Since the calculations carried out in order to determine the plastic volume are performed on an element basis, the nodal stresses supplied as input data to the algorithm could be either unaveraged element nodal stresses or, alternatively, nodal-averaged values. For the purposes of the numerical examples detailed in this report, nodal-averaged values are used. A choice also exists between interpolating nodal equivalent stresses or interpolating the complete stress tensor. The more appropriate approach is the latter and it is this that has been adopted for the numerical examples presented in this paper.

6. Numerical examples

This section is concerned with demonstrating that the scheme presented in this paper performs correctly and effectively i.e. in how the finite element estimate of the PVFE, F_h^e, approximates the exact PVFE, F^e. Additionally, as a way of developing an understanding of the PVFE quantity, the nature of the relationship between the F^e and the PVF, F, will be explored.

The first numerical example investigates a problem for which both F^e and F are known and demonstrates, for a range of finite element types, that the scheme presented in this paper is able to predict effectively the F^e.

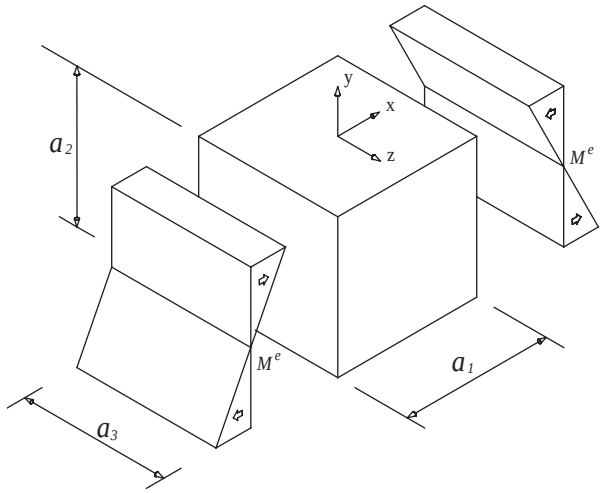

Fig. 11. Geometry and applied loading.

The second numerical example takes the case of plasticity in a thin rotating disc as an example exhibiting the sort of stress field found in rotating components.

In the third numerical example a centrifugal compressor impeller is examined.

6.1. Example number 1—cubic beam

This example has been chosen with the primary aim of demonstrating that the numerical scheme presented in this paper is convergent for a range of different types of three-dimensional continuum elements of the type typically found in commercial finite element codes. As with other quantities, the PVFE predicted by the finite element model, $\tilde{F}^{\mathrm{e}}_h$, should converge to the exact value, F^{e}, as the mesh is refined i.e.

$$\tilde{F}^{\mathrm{e}}_h \to F^{\mathrm{e}} \text{ as } h_{\max} \to 0, \tag{4}$$

where h is the characteristic length of an element in the finite element mesh and the subscript max indicates that the maximum elemental value is taken.

It is important, therefore, that the problem chosen possess an analytical, closed-form elastic solution from which the exact PVFE, F^{e}, can be determined. In addition, if the problem possess a closed-form plastic solution then comparison between the exact PVF, F, and the exact PVFE, F^{e}, may also be made.

A problem possessing closed-form solutions for both elastic and plastic stress fields is that of a rectangular parallelepiped geometry loaded on a pair of opposite faces, in the manner of a beam, with equal and opposite moments. The geometry and boundary conditions for the elastic stress field are shown in Fig. 11. The second moment of area for the beam is

$$I = \frac{a_3 a_2^3}{12}. \tag{5}$$

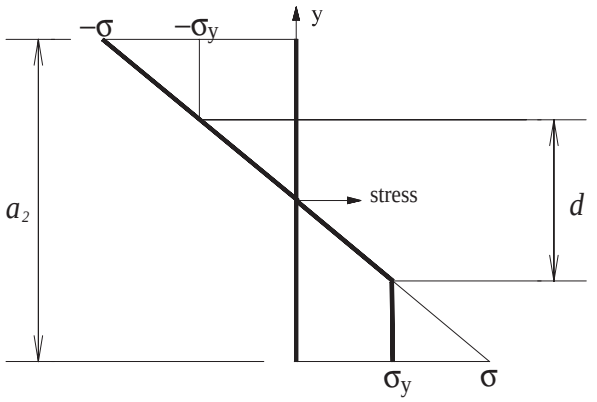

Fig. 12. Elastic and plastic stress distributions.

The closed-form elastic solution to this problem is a uniaxial stress field with linear variation in the y-direction as highlighted in the upper half of Fig. 12.

In the lower half of the figure the closed-form plastic solution, in which the stress is limited to the yield stress, σ_y, is highlighted. The parameter d is used to quantify the volume of material in which the stress remains below yield and, in conjunction with the dimension a_2 can be used to form the plastic volume fraction:

$$F = \frac{a_2 - d}{a_2}. \tag{6}$$

The applied moment, M, which is a function of the plastic volume fraction can be normalised in the following manner:

$$L = \frac{Ma_2}{12I\sigma_y}. \tag{7}$$

The normalised moment required to achieve a given plastic volume fraction with an elastic stress distribution can be deduced from Fig. 12 as

$$L^e = \frac{1}{6(1-F)}. \tag{8}$$

In a similar manner the normalised moment for a given plastic volume fraction with a plastic stress distribution is

$$L^p = \frac{2(1+F) - F^2}{12}. \tag{9}$$

The variations of plastic volume fraction with applied moment for both elastic and plastic cases are shown in Fig. 13. For the elastic case $F^e \to 1$ as $L \to \infty$. In contrast, for the plastic case a unit plastic volume fraction, $F = 1$, is achieved with a finite applied moment of $L = 1/4$.

This problem is now analysed by the finite element method using meshes consisting of regular grids of tetrahedral, pentahedral and hexahedral elements. A normalised moment of 1/3 is applied

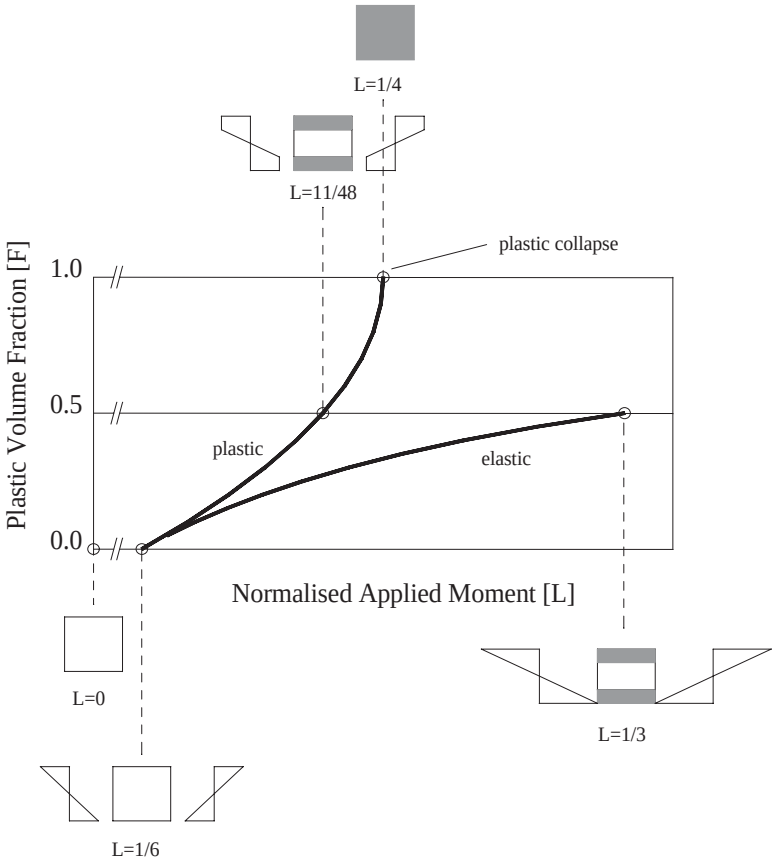

Fig. 13. Plastic volume fraction versus normalised applied moment.

so that the plastic volume fraction that should be recovered from the models is 1/2. Equal values are chosen for a_1, a_2 and a_3 such that the geometry is a cube. Both linear and quadratic elements are considered and, where the exact solution is not recovered with the initial mesh (level_0), up to two additional uniformly refined meshes, designated level_1 and level_2, are considered.

The way in which the various models perform is illustrated in Fig. 14 where carpet plots of unaveraged von Mises stress are presented. In this figure the darker shade is used to indicate regions where the finite element stress exceeds the yield stress. The figure lists the finite element approximation to the PVFE, F_h^e, and, in addition, presents the strain energy ratio R. This quantity, which is only possible to evaluate with a knowledge of the exact solution, provides an integral measure of proximity of the finite element solution to the exact value.

For this problem, in which the exact stress field is linear, meshes of all types of quadratic elements can reproduce the exact solution. Meshes of linear elements are capable only of approximating the exact solution and have strain energies that converge with (uniform) mesh refinement, as expected for force driven problems, from below the exact value. In most cases the estimated plastic volume fraction is seen to be close to the exact value i.e. $F_h^e \approx F^e$. This, however, is not the case for the coarse models of both linear and quadratic tetrahedra. There appear to be two reasons for this

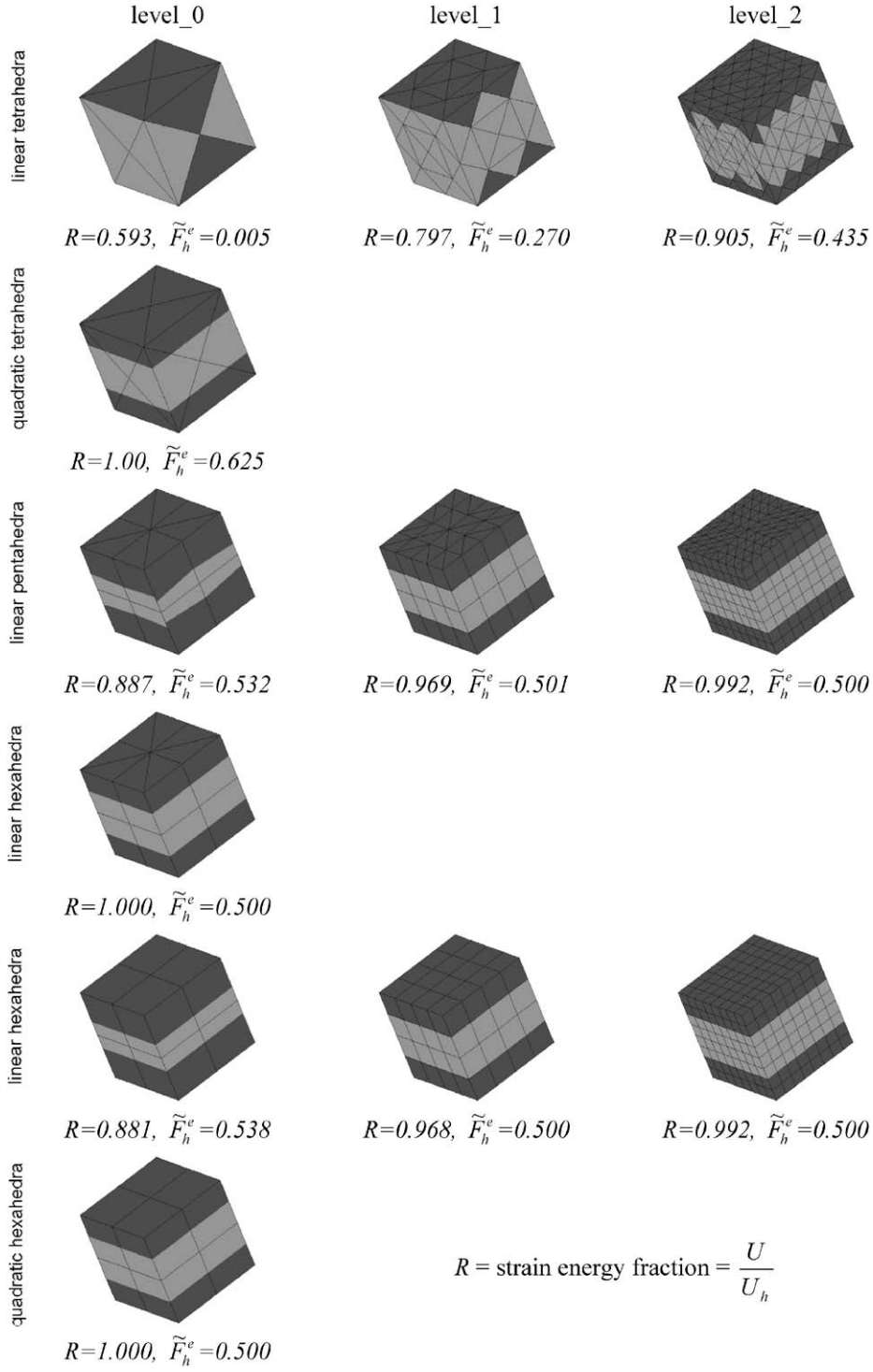

Fig. 14. Carpet plots of unaveraged von Mises stress.

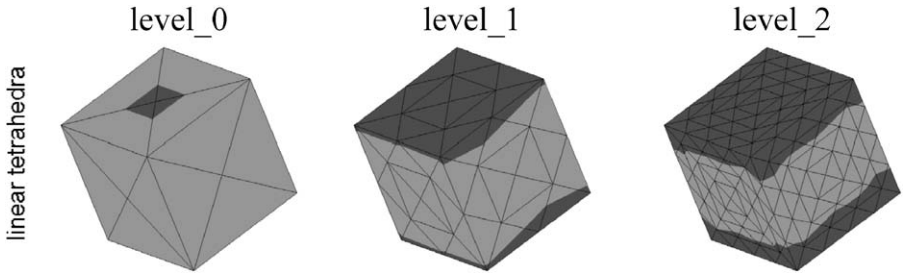

Fig. 15. Carpet plots of nodal -averaged von Mises stress.

observation as outlined below.

(1) With coarse models, especially of linear elements, the difference between averaged and unaveraged values can be significant as is demonstrated by comparing the results presented in the first row of Fig. 14 with those of Fig. 15 which have been averaged.
As discussed, nodal-averaged values have been used in the plastic volume calculations thus providing an explanation for the, initially, rather surprisingly small estimate of the plastic volume fraction for the level_0 and level_1 meshes of linear tetrahedra.
(2) The estimated plastic volume for the mesh of quadratic tetrahedra is greater than the true value even though the model reproduces the exact solution in terms of stresses. An explanation for this behaviour is provided through consideration of a one-dimensional analogue.

In Fig. 16 three cases of stress variation over a one-dimensional line element are considered. For each case, the actual stress distribution, σ, is drawn together with the modulus of the stress, $|\sigma|$, (this being representative of the von Mises stress in the three-dimensional situation) and a linearisation of the modulus of the stress $|\sigma|_L$ as used in the method of estimating the plastic volume currently under discussion.

The length of the line element in which the stress exceeds yield is termed the plastic length and for an element of uniform cross-section would be proportional to the plastic volume. It can be seen that the plastic length obtained when using the linearised stress can be significantly greater than that for the unlinearised stress field. The degree to which the plastic length is over-predicted is strongly case dependent and will only occur when the stress changes sign along the edge of an element as is the case for the mesh of quadratic tetrahedra used in the beam problem. Because of the higher degree of variation in stress within an individual element, it would appear that this behaviour is more likely to occur for quadratic elements and that it would tend to lead to a safe over-estimate of the plastic volume.

This example demonstrates the convergence of Eq. (4) and by doing so illustrates the convergent nature of the sampling scheme i.e. that $\tilde{F}_h^{\mathrm{e}} \to F_h^{\mathrm{e}}$ as $h_{\max} \to 0$.

6.2. Example number 2—thin rotating disc

Whilst the previous example served to demonstrate the convergence of the scheme for estimating the PVFE, the linear uniaxial stress field in the cube cannot really be considered as representative of

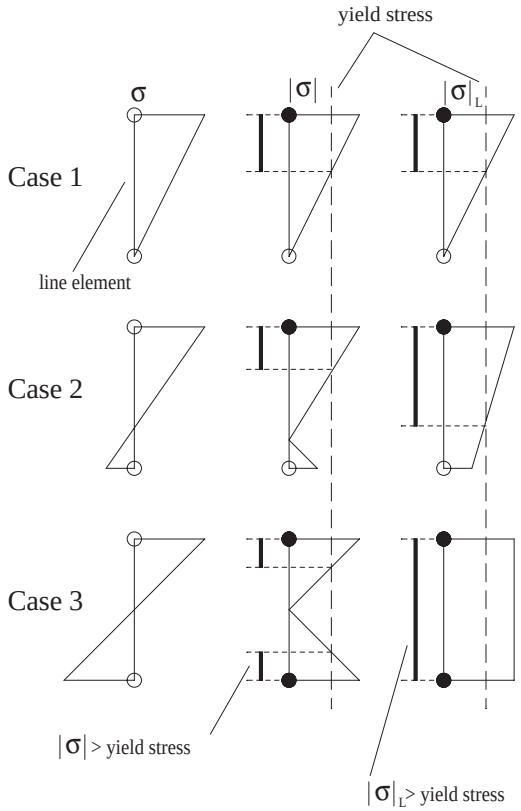

Fig. 16. Over-estimation of plastic volume—demonstration in 1D.

the sort of stress field occurring in rotating components. In contrast, this example, whilst effectively one-dimensional in nature, possesses a stress field which represents closely that which occurs in the hub and shroud of a centrifugal impeller.

As with example number 1, the thin (plane stress) rotating disc possesses closed-form solutions for both elastic and plastic stress fields and these are well known and widely reported for both steady-state conditions [7] and for accelerating conditions [8]. Whilst elastic and plastic closed-form solutions will be compared, the main objective of this example will be to establish how effectively the finite element estimates the PVFE in particular with the sort of coarse meshes that will be used for modelling the centrifugal impellers for which the scheme presented in this paper was developed.

For the disc being considered, the plastic volume fraction may be expressed in terms of the inner and outer radii, r_{i} and r_{o}, respectively, and the plastic interface radius r_p which is the radius at which the yield surface resides

$$F = \frac{r_{\mathrm{p}}^2 - r_{\mathrm{i}}^2}{r_{\mathrm{o}}^2 - r_{\mathrm{i}}^2}. \tag{10}$$

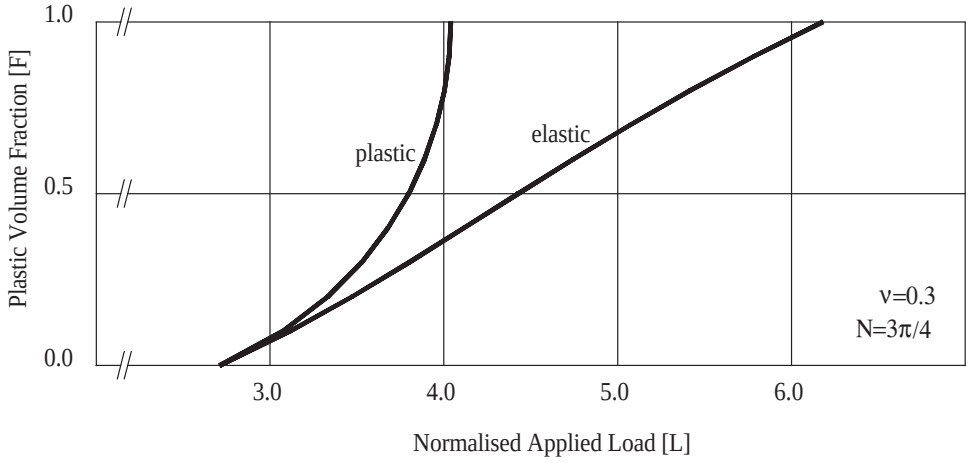

Fig. 17. Plastic volume fraction versus normalised applied load.

In addition to the plastic volume fraction, a further non-dimensional geometric parameter, here termed the *normalised area*, can be defined for the rotating disc

$$N = \frac{A}{r_o^2}, \tag{11}$$

where $A = \pi(r_o^2 - r_i^2)$ is the area of the generator plane of the disc.

As with the previous example, a non-dimensional applied loading term which is a function of the plastic volume fraction, the normalised area and Poisson's ratio can be defined as

$$L = \frac{\rho A \omega^2}{\sigma_y}. \tag{12}$$

Using the equations for the elastic stress distributions, as summarised in Appendix A to this paper, the normalised loading may be expressed as

$$L^e = \frac{12\pi N\{2\pi(D_1 - D_2)\}}{D_1\{8\pi^2 + N^2(3\nu + 1)(F-1)^2\} - 4D_2\{\pi - N\}}, \tag{13}$$

where $D_1 = \sqrt{\{\pi + N(F-1)\}}$ and $D_2 = \{2\pi + N(F-1)\}\sqrt{(\pi - N)}$.

In a similar manner, using the expressions for the plastic stress distribution derived using the Tresca yield criterion, the normalised loading may be written as

$$L^p = \frac{8\pi N\{\pi + N(F-1)\}}{8\pi^2 - 2\pi N\{2F(\nu-1) - \nu + 5\} - N^2\{F(3\nu+1) - 2(\nu-1)\}\{F-1\}}. \tag{14}$$

Representative, i.e. for a given values of N and ν, variations of plastic volume fraction with applied load for both elastic and plastic cases are shown in Fig. 17. In contrast to the first example, where an infinite moment was required to obtain a unit PVFE, $F^e = 1$ is achieved with a finite applied load for the rotating disc.

An axisymmetric finite element model of a disc is now considered. The finite element mesh of the generator plane in which the dimensions of the disc are identified is shown in Fig. 18. A

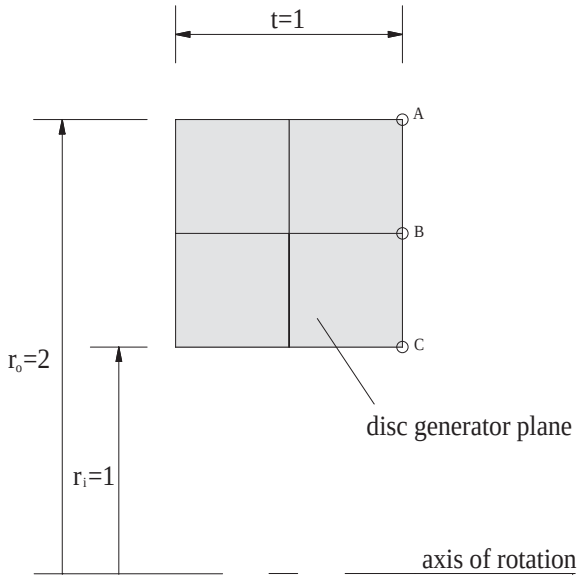

Fig. 18. Finite element mesh for thin rotating disc.

square generator plane has been used in order to avoid element distortion whilst retaining a coarse four-element mesh. The thickness of the model is such that in the centre of the model the plane stress assumption is invalid. The stresses at the outer axial positions A, B and C in Fig. 18, however, will adhere to the plane stress assumption and it is these that will be used in the ensuing discussion. Although results will only be reported at the corner nodes identified in the figure, eight-noded elements with mid-side nodes were used in the analysis.

The material and mechanical properties chosen for this analysis were those of a typical steel:

$$E = 210 \text{ GPa}, \ v = 0.3, \ \rho = 7800 \text{ kg/m}^3, \ \sigma_y = 200 \text{ MPa}. \tag{15}$$

The angular velocity used for the analysis was set to correspond with a PVFE of $F^e = 0.5$ which was calculated using Eq. (A.4) (see Appendix A) as $\omega = 109.749$ rad/s. It is noted that although at this speed the disc would in practice be fully plastic, with an area-mean hoop stress of 219.22 MPa (calculated using Eq. (A.5)), for a typical steel, which will have a tensile strength significantly above this level of stress, the disc would not have failed through bursting [9].

In this example the Tresca yield criterion is used [7]. For the thin rotating disc $\sigma_\theta > \sigma_r$ for all radii, r, and based on the Tresca yield criterion the equivalent stress is

$$\sigma_{eq} = \sigma_\theta - \sigma_r. \tag{16}$$

The stresses as reported by the finite element model at the points identified in Fig. 18 are listed in Table 1 along with the corresponding equivalent stress.

Assuming a linear variation of equivalent stress between element corner nodes the radial position of the yield surface can be determined ($r_p = 1.63$) and the corresponding PVFE is calculated to be $\tilde{F}_h^e = 0.55$. For this example it is observed, therefore, that the finite element method over-estimates the true PVFE.

Table 1
Finite element stresses [MPa]

Point	σ_θ	σ_r	σ_{eq}
A	140.4	3.3	137.1
B[a]	205.9	41.9	164.0
C	314.1	12.0	302.1

[a]nodal averaged results are reported for this position.

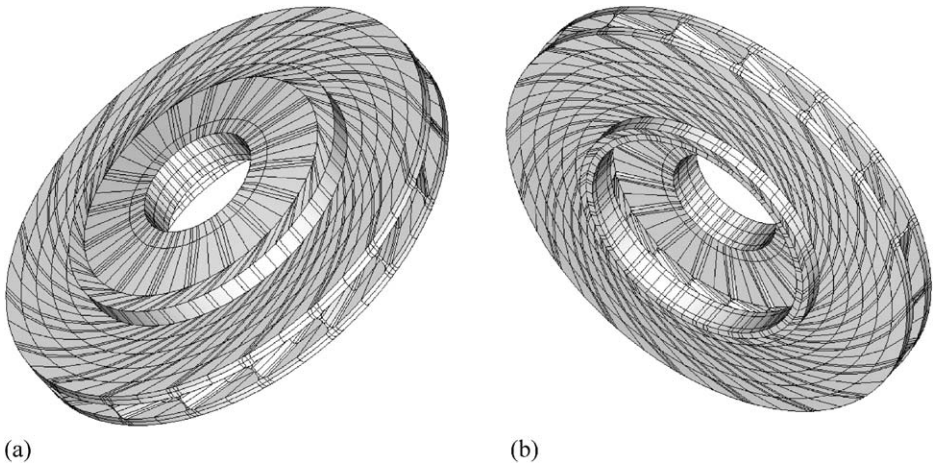

Fig. 19. Finite element mesh for centrifugal impeller—full wheel.

6.3. Example number 3—centrifugal impeller

This third and final problem has been included as an example of the intended application of the method. A full-wheel model of a low flow coefficient centrifugal compressor wheel, of the sort discussed in Ref. [10] is shown in Fig. 19. For a study of the stresses induced by centrifugal loading alone, it is sufficient to consider a cyclically symmetric sector model.

The study conducted here will involve monitoring the way in which the plastic volume fraction varies with yield stress and the results, generated using higher-order elements, are shown in Fig. 20 in which carpet plots of nodal-averaged von Mises stress are plotted for selected values of yield stress. In order to normalise the yield stress, it has been divided by the maximum von Mises stress occurring in the model and is given the symbol S. The contour levels are adjusted for each case so that the darker shading represents regions where the von Mises stress exceeds yield.

For values of the normalised yield stress of zero and unity the exact plastic volume fractions are known. For intermediate values of S the plastic volume fraction varies smoothly between 1 and 0 as shown in the figure. The regions in which plasticity first appears are those occurring around the leading edge of the impeller. Plasticity then progresses into the shroud and finally into the hub of the impeller. If the aim is to limit plasticity to the leading edge where an improved fatigue life

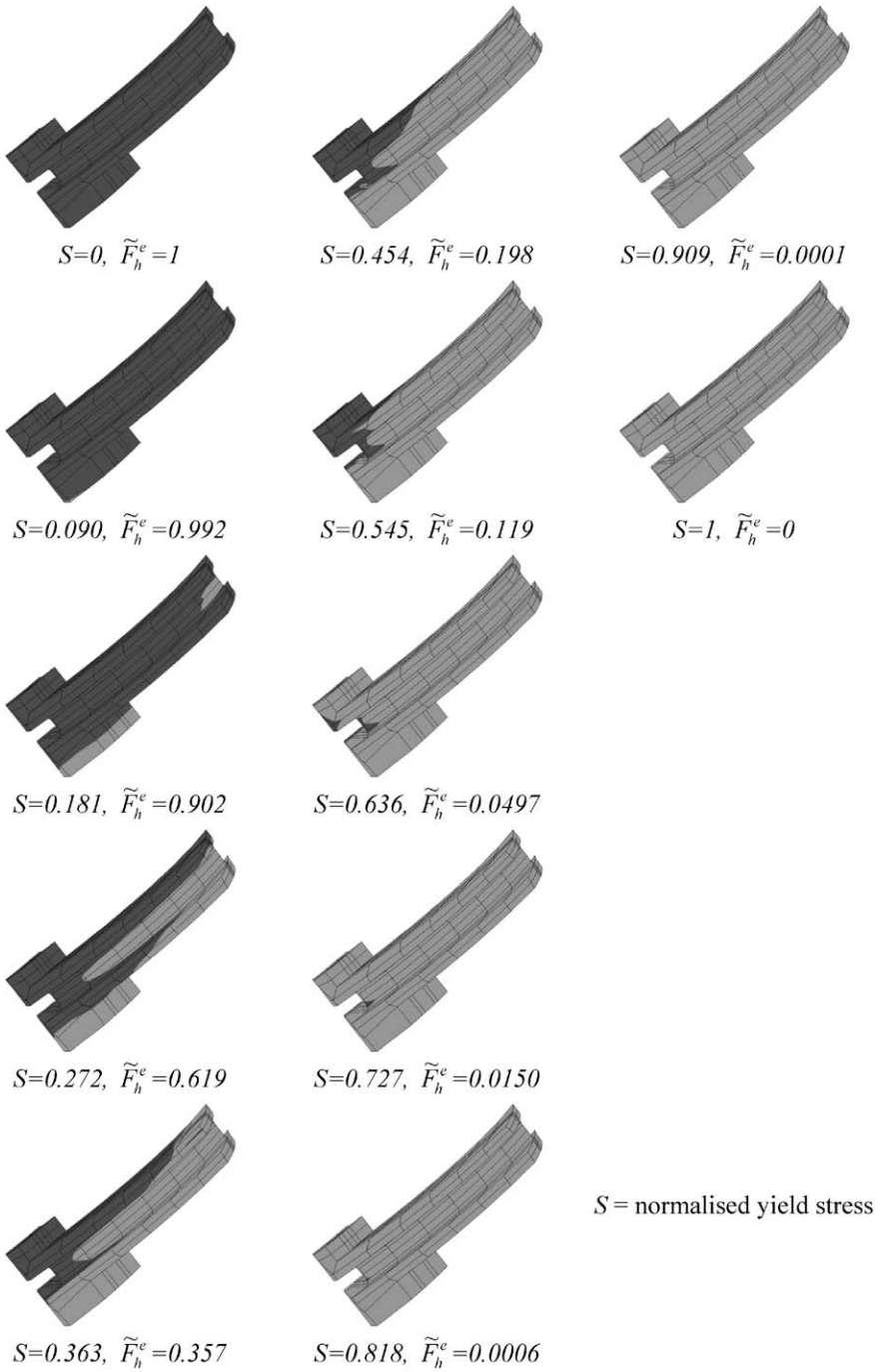

Fig. 20. Carpet plots of nodal averaged von Mises stress—sector model.

is desirable and to ensure that plasticity does not progress to the shroud where tolerances in the regions of sealing rings are of importance then, for the impeller being considered here, a plastic volume fraction in the region of 0.05 might be considered acceptable. This value of the plastic volume fraction is of the order of magnitude used in the industry and can be seen as appropriate by inspection of the plots of plastic volume fraction versus applied load for examples 1 and 2 (Figs. 13 and 17, respectively). There it is seen that whilst the elastic and plastic curves are diverging, the error in applied load between the two curves for a plastic volume fraction of 0.05 is small.

Whilst not proposed as a general finding, the results of examples number 1 and 2 indicate the behaviour of the various quantities to be characterised by the following inequality:

$$F \geqslant \tilde{F}_h^{\mathrm{e}} \geqslant F^{\mathrm{e}} \tag{17}$$

It is also demonstrated that for small plastic volume fractions $F^{\mathrm{e}} \to F$. It is reasonable to assume, therefore, that for plastic volume fractions of the magnitude likely to be used for the impeller, the finite element approximation is close to the true value.

7. Closure

A scheme for estimating the plastic volume fraction based on the results of a linear-elastic finite element analysis has been presented. The scheme has been designed for use with coarse meshes in which it is necessary to account for the variation in stress within a single element. The computational effort required by the scheme is not significant being comparable to other post-processing operations that manipulate element stress fields. The convergence of the scheme has been examined and the relationship between the plastic volume fraction as calculated from a plastic stress field (PVF) and that calculated from an elastic stress field (PVFE) has been investigated.

The PVFE is a quantity that is used in the assessment of centrifugal impellers and an example of this has been provided in this paper. Limiting values for this quantity derive from long experience gained from the design of similar components and a realisation that for small amounts of plasticity the PVFE closely approximates the true value. Whilst values are likely to be application dependent, the examples shown in this paper indicate that a plastic volume fraction of 0.05 is a not unreasonable limiting value for the validity of the linear-elastic approximation. The development of the scheme presented in this paper has enabled the automation of what was previously a manual process thereby allowing structural constraints to be checked automatically within a computational system for the automatic optimisation of impeller geometries.

Acknowledgements

The work reported in this paper is part of a collaboration between PCA Engineers Limited, Sulzer Turbo[3] and Sulzer Innotec.[4] The author would like to record his gratitude to Dr. Ayten Genç for identifying the relevant theoretical basis for defining combinations of nodal stress configurations, to

[3] Sulzer Turbo Limited, Zurich, Switzerland.

[4] Sulzer Innotec Limited, Winterthur, Switzerland.

Mr. Peter Came for advice generously given during the preparation of the introduction, and to the reviewers for their helpful comments.

Appendix A. Equations for rotating discs

The stresses in the elastic portion of a thin rotating disc are

$$\sigma_r = C_1 + \frac{C_2}{r^2} - \frac{3+v}{8}\rho\omega^2 r^2, \quad \sigma_\theta = C_1 - \frac{C_2}{r^2} - \frac{1+3v}{8}\rho\omega^2 r^2, \tag{A.1}$$

where the constants of integration C_1 and C_2 are determined from the (radial) stress free conditions at inner and outer radius as

$$C_1 = \frac{3+v}{8}\rho\omega^2(r_i^2 + r_o^2), \quad C_2 = \frac{3+v}{8}\rho\omega^2 r_o^2 r_i^2. \tag{A.2}$$

The radial position of the yield surface, $\tilde{r}_p$, according to the Tresca yield criterion is determined by solving the following equation:

$$\sigma_\theta = \sigma_y, \quad r = r_p \tag{A.3}$$

and for a given radius r_p the angular velocity is

$$\omega^e = \sqrt{\frac{-8\sigma_y r_p^2}{\rho\left(r_p^4(3v+1) - r_p^2 D_0(v+3) - D_1(v+3)\right)}}, \tag{A.4}$$

where $D_0 = r_i^2 + r_o^2$ and $D_1 = r_i^2 r_o^2$.

The area-mean hoop stress is traditionally used in disc design to ensure adequate burst margin and is defined as

$$\bar{\sigma}_\theta = \frac{\int_A \sigma_\theta \, dA}{\int_A dA}, \tag{A.5}$$

where A is the area of the disc generator plane.

Carrying out the integration of Eq. (A.5) on the uniform thickness disc under consideration leads to

$$\bar{\sigma}_\theta = \frac{\rho\omega^2}{3}\frac{(r_o^3 - r_i^3)}{(r_o - r_i)}. \tag{A.6}$$

References

[1] P.M. Came, C.J. Robinson, Centrifugal compressor design, Proceedings of the Institution of the Mechanical Engineers, Part C, J. Mech. Eng. Sci. 213 (C2) (1999) 139–155.

[2] A. Nadai, L.H. Donnell, Stress distributions in rotating discs of ductile material after the yield point has been reached, Trans. ASME 51 (1929) 173–181.

[3] D.G. Wilson, T. Korakianitis, The Design of High-Efficiency Turbomachinery and Gas Turbines, 2nd Edition, Prentice-Hall, Englewood, Cliffs NJ, 1998, p. 556.

[4] R.V. Hogg, J. Ledolter, Applied Statistics for Engineers and Physical Scientists, 2nd Edition, Macmillan Publishing Company, New York, 1992.
[5] J. Robinson, Understanding Finite Element Stress Analysis, 2nd Edition, ISBN 0-9507-172-0-7, Robinson and Associates, Bridestowe, UK, 1981.
[6] J.A. Collins, Failure of Materials in Mechanical Design: Analysis, Prediction, Prevention, John Wiley & Sons, New York, 1993.
[7] D.W.A. Rees, Elastic-plastic stresses in rotating discs by von Mises and Tresca, Z. Angew. Math. Mech. 79 (4) (1999) 281–288.
[8] T. Reddy, A. Yella, H. Srinath, Effect of acceleration stresses on the yielding of rotating disks, Int. J. Mech. Sci. 16 (1974) 593–596.
[9] A.G. Holms, J.E. Jenkins, Effect of strength and ductility on burst characteristics of rotating discs, Natl. Adv. Comm. Aeron., Tech. Note 1667, 1948.
[10] P. Dalbert, B. Ribi, T. Kmeci, M.V. Casey, Radial compressor design for industrial compressors. Proceedings of the Institution Mechanical Engineers, Part C, J. Mech. Eng. Sci. 213 (C2) (1999) 71–83.